Communications Earth & Environment https://doi.org/10.1038/s43247-026-03420-3

Article in Press

Sulfur isotope heterogeneity in Martian shergottites reveals early atmosphere - mantle exchange

Received: 9 September 2025

Accepted: 10 March 2026

Cite this article as: Patil, K., Dottin, J.W., Fu, H. *et al.* Sulfur isotope heterogeneity in Martian shergottites reveals early atmosphere - mantle exchange. *Commun Earth Environ* (2026). https://doi.org/10.1038/s43247-026-03420-3

Kiran Patil, James W. Dottin III, Hairuo Fu, Brian Monteleone, Nilanjan Chatterjee, Noah Hooper, Gareth Izon, J. Cameron Adams, Anthony Irving, Charles K. Shearer, Heather B. Franz & Shuhei Ono

Sulfur isotope heterogeneity in Martian shergottites reveals early atmosphere - mantle exchange

Kiran Patil[1*], James W. Dottin III[1], Hairuo Fu[1], Brian Monteleone[2], Nilanjan Chatterjee[3], Noah Hooper[1], Gareth Izon[3], J. Cameron Adams[1], Anthony Irving[4], Charles K. Shearer[5], Heather B. Franz[6], Shuhei Ono[3]

[1]*Department of Earth, Environmental and Planetary Sciences, Brown University, Providence, RI, USA*
[2]*Marine Geology and Geophysics Department, Woods Hole Oceanographic Institution, Woods Hole, MA, USA*
[3]*Department of Earth, Atmospheric, and Planetary Sciences, Massachusetts Institute of Technology, Cambridge, MA*
[4]*Department of Earth and Space Sciences, University of Washington, Seattle, WA, USA,*
[5]*Earth and Planetary Sciences Department, University of New Mexico, Albuquerque, NM, USA*
[6]*Goddard Space Flight Center NASA, Greenbelt, MD, USA*

*Corresponding author. Email: kiran_patil@brown.edu

Abstract

The study of sulfur isotopes on Mars provides crucial insights into the planet's formation, differentiation, and volatile evolution. Primordial sulfur isotope compositions help distinguish Martian sulfur sources, including core-mantle interactions, magmatic outgassing, and atmospheric cycling. While bulk analyses have shown limited mass-independent fractionation (MIF-S), the mechanisms introducing MIF-S into Martian magmas remain poorly understood. Using in situ secondary ion mass spectrometry (SIMS), we analysed sulfides in four shergottites: Yamato 980459, Tissint, Gadamis 001, and NWA 11300, and found extreme heterogeneity in $\Delta^{33}S$ (–1.3 ± 0.48‰ to +1.42 ± 0.64‰) and $\delta^{34}S$ (–3.5 ± 0.11‰ to +0.73 ± 0.15‰). Large $\Delta^{33}S$ anomalies are observed in both depleted and enriched samples, indicating that MIF-S sulfur was incorporated

into Martian magmatic systems through prolonged mantle-atmosphere exchange. This exchange likely began during magma ocean crystallisation and continued into later magmatic stages through ingassing, crustal assimilation, and/or recycling of crustal sulfur.

Introduction

Sulfur is a siderophile, chalcophile and volatile element which makes it a particularly powerful tool for reconstructing early solar system processes and planetary differentiation. During solar system formation, gaseous sulfur species in optically thin regions of the solar nebula, were susceptible to photochemical reactions that could have imprinted mass-independently fractionated sulfur (MIF-S) signatures [1–3]. MIF-S is readily observed among a variety of sulfur bearing minerals in carbonaceous chondrites [4] and achondrites from differentiated planetesimals. While chondritic and achondritic materials demonstrate that MIF-S production occurred in the solar nebula, the MIF-S signatures among achondrites highlights that the MIF-S signatures are preserved in planetary cores, at their core-mantle boundaries, and in their silicate mantles [4–6]. However, similar nebular components have not yet been identified among materials from the Earth, Moon, or Mars.

As the terrestrial planets formed, they likely experienced magma ocean phases [7,8], during which sulfur, along with other volatiles, may have been processed and fractionated [9]. On Earth, material associated with the core and core-mantle boundary has been identified in lavas that sample deep rooted mantle plumes [10–12]. However, the relatively large abundance of sulfur in the mantle and lack of isotopic fractionation at high temperatures and pressure [13–15], complicates efforts to identify a clear nebular sulfur component of Earth. Additionally, homogenization and/or overprinting of early sulfur isotope signatures through nearly 4.5 billion years of mantle convection and recycling of subducted surface material further obscures any primordial sulfur signal [16,17]. In contrast, Mars,

with its comparatively limited and episodic volcanic activity, may have preserved primordial sulfur components. Therefore, materials from Mars provides a unique opportunity to (1) evaluate whether the terrestrial planets received similarly exogenous nebular or atmospheric sulfur, and (2) assess the degree of sulfur homogeneity in the Martian mantle [18].

Martian meteorites are the only available physical samples from Mars. Excluding Martian polymict breccias and orthopyroxenite Allan Hills 84001, the meteorites are classified as shergottites, nakhlites, and chassignites, which represent basaltic to gabbroic rocks (shergottites), clinopyroxene-rich cumulates (nakhlites), and olivine-rich cumulates (chassignites), respectively. Among these, shergottites represent some of the most depleted Martian mantle-derived rocks and can be further sub-divided based on their trace element and isotopic characteristics. Depleted shergottites are characterised by low bulk rare earth element patterns with $(La/Yb)_{Cl} < 0.3$, low initial ratios of $^{87}Sr/^{86}Sr$, $^{207}Pb/^{204}Pb$, $^{206}Pb/^{204}Pb$, $^{208}Pb/^{204}Pb$, and $^{187}Os/^{188}Os$, as well as elevated initial $^{142}Nd/^{144}Nd$, $^{143}Nd/^{144}Nd$, and $^{176}Hf/^{177}Hf$ ratios, reflecting a relatively primitive mantle source [19]. In contrast, enriched shergottites, are characterised by high bulk rare earth element patterns with $(La/Yb)_{Cl} > 0.8$ and display geochemical trends that are opposite to that observed in depleted shergottites, which reflects derivation from an enriched or metasomatized mantle reservoir [19]. Bulk sulfur isotope analyses of shergottites generally show non-mass dependent $\Delta^{33}S$ signatures [18,20–22]. Since the shergottite derived bulk sulfur isotope composition of the Martian mantle does not differ significantly from its assumed primordial value ($\delta^{34}S = 0‰$, $\Delta^{33}S = 0‰$), $\Delta^{33}S$ anomalies are interpreted as a secondary feature that are linked to processes that occurred throughout Mars' evolution. Consequently, the observed large $\Delta^{33}S$ anomalies in nakhlites and polymict breccias (e.g., NWA 7034) are attributed to assimilation of sulfur that was photochemically processed in the early Martian atmosphere [18,23–28]. Therefore, the lack of MIF-S

in most shergottites is argued to reflect limited assimilation of atmospheric sulfur. However, the current estimate for the sulfur isotopic composition of the Martian mantle excludes a few analyses of geochemically enriched shergottites (e.g., Gadamis 001, NEA 001) that display anomalous $\Delta^{33}S$ values [22]. The heterogeneity in $\Delta^{33}S$ among the enriched shergottites is explained by the possible incorporation of atmospherically processed sulfur among basaltic shergottites that crystallized in the shallow subsurface [22]. However, combined petrologic and isotopic evidence that supports this hypothesis has not yet been reported. Without this information, it remains possible that the MIF-S signature was a component of the erupted melt rather than an assimilated component.

To constrain whether all MIF-S signatures in shergottites are the result of post/syn-eruptive crustal assimilation versus a component of the original erupted melt, a detailed in-situ S isotope approach is needed. While bulk sulfur isotope analyses provide constraints on the nature and composition of sulfur that dominates the lava from which the respective meteorites derive, they mask potential intergranular compositional heterogeneity. Since sulfide occurs both in mesostasis and as inclusions within mafic phenocrysts in Martian meteorites, it is plausible that multiple distinct sulfur components were captured during the crystallisation of the respective melts, which would complicate proper interpretations of the bulk S isotope data published thus far. Therefore, to complement the existing bulk S isotope analyses, this study reports *in situ* sulfur isotope measurements of individual sulfide grains among four shergottites: Yamato 980459 (or Y98), Tissint, Gadamis 001, and NWA 11300, with geochemical characteristics indicative of variably incompatible trace element enriched (or depleted) reservoirs (see Supplementary Text for more detailed description of the samples). The possibility of two (or more) distinct sulfur components in Martian meteorites provides an opportunity to evaluate the relative homogeneity of $\Delta^{33}S$

estimates in the Martian mantle and to determine whether sulfur isotopes can help constrain the petrogenesis of the Martian mantle. This study seeks to use the geochemically diverse samples to determine whether the processes of geochemical enrichment are linked to the processes associated with MIF-S delivery to martian meteorites. Such insights can provide constraints on the processes associated with establishing the volatile abundances among depleted and enriched mantle sources on Mars while ultimately linking S isotope compositions to a specific petrogenic model among variably enriched Martian meteorites.

Results

Sulfides present as troilite, Ni rich – pyrrhotite, and pentlandite were identified (Table 1) and analysed for triple S isotopes. The sulfur isotope results of n = 40 analyses across n = 29 sulfides in shergottites are reported in Table 2. The data exhibit extreme heterogeneity in $\delta^{34}S$ (~ –3.5 to +0.7‰) and $\Delta^{33}S$ (–1.3 to +1.4‰, 2 S.D.) (Fig. 1). These values contrast sharply with those reported using bulk sulfur isotope techniques, which yield $\delta^{34}S$ values of –0.88 to +0.84‰ (±0.3‰) and $\Delta^{33}S$ values ranging from –0.032 to +0.37‰ (±0.016‰) (Fig. 2, Fig. 3) [18,21,22]. Sulfides that show the largest $\Delta^{33}S$ anomalies in the analysed samples are shown Fig. 4. For more detailed SIMS results, see the Supplementary Results. To ensure the reliability of the SIMS data, several quality-control measures were implemented. These include plots demonstrating the absence of correlations between MIF-S anomalies and sulfide textures, as well as Fe, Ni, S, and Cu concentrations (see Supplementary Figures S2–S4 and S15). In addition, pre- and post-SIMS optical microscope and electron microprobe images of the analysed sulfides are provided in Supplementary Figures S6-13 and S17.

Tissint

Sulfur isotopes in Tissint sulfides show large variability, with $\delta^{34}S$ values from –1.79 ± 0.13 ‰ to 0.28 ± 0.12 ‰ (2σ) and $\Delta^{33}S$ from –0.34 ± 0.57 ‰ to 0.52 ± 0.58 ‰ (2σ), even among sulfides within the same phenocryst. Most $\Delta^{33}S$ values deviate from the solar system reference (canyon diablo troilite) ($\Delta^{33}S = 0$ ‰), though two sulfides ($\Delta^{33}S \approx 0$ ‰) align with this composition. Sulfides occur as mineral inclusions rather than within impact melt. Bulk isotopic values ($\delta^{34}S$ = –0.82 ± 0.3 ‰; $\Delta^{33}S$ = 0.024 ± 0.008 ‰) are similar to the SIMS results, indicating that the analyses are representative of the whole rock.

Yamato 980459 (Y98)

All Y98 sulfides display positive $\Delta^{33}S$ (0.24 ± 0.67 to 0.61 ± 0.48 ‰ (2σ)) and negative $\delta^{34}S$ (–2.91 ± 0.12 to –0.15 ± 0.19 ‰ (2σ)) values. SIMS data are biased toward mesostasis-hosted sulfides, as those in olivine and pyroxene were too small for analysis. Consequently, SIMS results differ from bulk values ($\delta^{34}S$ = –0.18 ± 0.3 ‰; $\Delta^{33}S$ = 0.006 ± 0.008 ‰, 2σ) and are not representative of the whole rock.

Gadamis 001

Gadamis sulfides show the most variability in $\Delta^{33}S$ as $\Delta^{33}S$ ranges from –1.31 ± 0.48 ‰ to 1.42 ± 0.64 ‰ (2σ), the largest anomaly among all shergottites. Positive $\delta^{34}S$ values predominate (mostly ~0.5 ‰) with limited variability. The highest $\Delta^{33}S$ values are linked to sulfides in shocked pyroxene, while the lowest occur in maskelynite. Bulk and SIMS measurements ($\delta^{34}S$ = 0.03 ± 0.3 ‰; $\Delta^{33}S$ = 0.19 ± 0.008 ‰, (2σ)) closely align, which indicates that the SIMS data are representative of the bulk rock. In Gadamis 001, the analysed sulfides occur as primary magmatic phases. Grains exhibiting anomalous $\Delta^{33}S$ values show no evidence of terrestrial weathering. The sample lacks secondary oxidation products (e.g., iron oxyhydroxides), terrestrial sulfates or

carbonates, and hydration features typically associated with alteration on Earth. Consequently, the large $\Delta^{33}S$ values are interpreted as Martian in origin and unrelated to terrestrial processes.

NWA 11300

Sulfides in NWA 11300 have $\Delta^{33}S$ values from –0.79 ± 0.52 ‰ (2$\boldsymbol{\sigma}$) to 0.53 ± 0.48 ‰ (2$\boldsymbol{\sigma}$) and $\delta^{34}S$ from –3.43 ± 0.27 ‰ (2$\boldsymbol{\sigma}$) to 0.61 ± 0.19 ‰ (2$\boldsymbol{\sigma}$). Most analysed grains are hosted in clinopyroxene and shocked glass, often containing oxide inclusions. The most negative $\delta^{34}S$ (–3.43 ± 0.11‰, (2$\boldsymbol{\sigma}$)) is the lowest recorded in a shergottite. Bulk isotopic compositions ($\delta^{34}S$ = 0.28 ± 0.3 ‰; $\Delta^{33}S$ = –0.032 ± 0.016 ‰, (2$\boldsymbol{\sigma}$)) differ markedly from SIMS results, reflecting limited and inclusion-rich sampling.

Discussion

Characterising the Sulfur Isotope Composition of the Primitive Martian Mantle

Understanding the origin of MIF-S anomalies in shergottites requires first constraining the sulfur isotope composition of the primitive Martian mantle. Among the four samples examined in this study, Tissint and Y98 represent the most primitive Martian melts[29–32] and offer an opportunity to use S isotope measurements of their respective sulfides to obtain key insights into the baseline sulfur isotope characteristics of Mars's interior.

Y98 exhibits resolvable anomalies in both $\Delta^{33}S$ and $\delta^{34}S$. The measured anomalous values are different from the previously reported bulk sulfur isotope composition of Y98. In contrast, the lack of no resolvable $\Delta^{33}S$ anomalies in Tissint agrees with earlier work that suggests the bulk $\Delta^{33}S$ of the Earth, Moon, and Mars is near 0.00‰ [18,33,34]. However, a long-standing debate persists regarding the $\delta^{34}S$ composition of the primitive mantle of these planetary bodies. The $\delta^{34}S$ values

in Tissint are not homogeneous and deviate from what would be expected for a sulfur source derived from a fully homogenized mantle ($\delta^{3}S \approx 0‰$). The most negative $\delta^{34}S$ values in Tissint overlap with values estimated from bulk analysis[18], yet the spread in $\delta^{34}S$ likely reflects additional isotopic fractionation or mixing processes that have overprinted an initially uniform mantle signature that was established through core formation or early mantle differentiation[33,35].

$\delta^{34}S$ Variability and Evidence for Multiple Mantle Sources on Mars

The variability in $\delta^{34}S$ among shergottites provides an important window into the sulfur isotope evolution of the Martian mantle. While most $\delta^{34}S$ values range between −2‰ and +1‰, the statistically distinct values point to two compositional endmembers that indicate the possible involvement of at least two isotopically distinct sulfur reservoirs. Several processes have been proposed to explain the $\delta^{34}S$ variability among the shergottites, including magmatic degassing [36,37], mixing among an endmember established through isotopic fractionation during core formation[33,35] and a crustal component, and mixing between multiple accreted sulfur sources[15]. Magmatic degassing is unlikely to be the primary control on the observed sulfur isotopic and compositional variations, as no correlation is observed between sulfur concentration and $\delta^{34}S$ (Supplementary Figure. S5 and Supplementary Dataset S2)[22]. Additionally mixing between multiple accreted sulfur sources is unlikely as the $\delta^{34}S$ of analysed solar system materials is limited (~ -0.5‰ to +0.5‰). However, mixing among an endmember established through isotopic fractionation during core formation[33,35] and a crustal component remains a viable solution. The observed $\delta^{34}S$ range can be explained by a fractionation-mixing model (FMM) synonymous to an assimilation-fractional crystallisation (AFC) framework (Fig 5.) (details on the modelling parameters are provided in the Supplementary Discussion and Supplementary Dataset S3.) In this interpretation, Tissint (which

best represents the isotopic composition of a depleted mantle melt among our analysed sample suits) approximates the starting $\delta^{34}S$ value of the Martian mantle directly following differentiation and crystallisation. Perhaps, coincidently, the most negative $\delta^{34}S$ values are similar to the existing estimates for the primordial BSE and BSM[15]. Therefore, this isotopically light sulfur signature could reflect early metal-silicate segregation during core formation or the accretion of isotopically light planetesimals, consistent with the $\delta^{34}S$ range of the terrestrial and lunar mantle[15]. In our FMM, we hypothesise that as the Martian magma ocean crystallised and mantle reservoirs evolved, $\delta^{34}S$ values shifted toward isotopically heavier compositions (up to +1‰), best exemplified by enriched shergottites such as Gadamis 001. The positive $\delta^{34}S$ values in these samples resemble those observed in evolved lunar basalts, where similar $\delta^{34}S$ enrichment has been attributed to late-stage magma ocean crystallisation and internal redox-driven isotopic fractionation[33,38]. Together, the coexistence of isotopically light $\delta^{34}S$ in depleted shergottites and heavier $\delta^{34}S$ in enriched shergottites suggest that Mars hosts at least two isotopic and genetic mantle sulfur components.

Constraining the Mechanism of Anomalous Sulfur Incorporation in Shergottites

The observed heterogeneity in $\Delta^{33}S$ among analysed shergottites adds complexity to the existing understanding of the Martian sulfur cycle and the formation of primitive Martian melts. To account for the observed $\Delta^{33}S$ anomalies in shergottites, several possible mechanisms must be considered: i) assimilation of MIF-S reservoir during shallow crustal crytsallisation; ii) inheritance of isotopic heterogeneity from a primordial, nebular source; iii) addition of isotopically anomalous sulfur via carbonaceous chondrite-like impactors; iv) the existence of a MIF-S reservoir within the Martian mantle, established through early atmosphere-mantle interaction.

Crustal Assimilation as a Mechanism for Introducing MIF-S to Martian Magmas

Previous models have largely relied on crustal assimilation to explain the small MIF-S anomalies identified through bulk sulfur isotope analyses of shergottites[18,22]. In this framework, ascending magmas acquire isotopically anomalous sulfur through interaction with photochemically processed crustal materials, which can contribute non-zero $\Delta^{33}S$ values. Isotopic evidence for crustal assimilation has been well documented among nakhlites and several enriched shergottites [18,23–28]. Crustal assimilation, in principle, can account for the anomalies observed in some of our samples, particularly Gadamis 001 (enriched) and NWA 11300 (intermediate), which display resolvable $\Delta^{33}S$ deviations consistent with the assimilation of crustal sulfur. However, it is unclear whether there is strong petrographic support for this process having occurred among Gadamis 011 and NWA 11300.

Nakhlites display large and well-resolved MIF-S anomalies (identified through both in situ and bulk analyses)[23,24,28,39]. In nakhlites, petrographic evidence shows sulfides commonly occurring within the mesostasis in close association with titanomagnetite, and isotopic data from different sulfur species (i.e., sulfide vs. sulfate) indicate interaction with an oxidising agent[23,26–28]. Furthermore, Mari et al., 2019 and Day et al., 2024 show that larger MIF-S anomalies are associated with elevated $^{187}Os/^{188}Os$ (Fig 6) and this relationship has been used as additional evidence that Nakhlites assimilated crust with MIF-S[26,28].

In an attempt to apply a similar framework as Day et al., 2024 and Mari et al., 2019 to test for crustal assimilation in our sample suit we find that this approach cannot be applied to Tissint, Gadamis 001 and NWA 11300, as Tissint shows no resolvable MIF-S anomalies and $^{187}Os/^{188}Os$ data is unavailable for Gadamis 001 and NWA 11300. Y98 presents a more complex case. Although Y98 exhibits a texture similar to nakhlites, it lacks the accompanying LREE enrichment

or radiogenic Os signatures (Fig. 6) that are typical fingerprints of crustal contamination[26,28,29,40,41]. However, Y98's isotopic and geochemical characteristics are not consistent with assimilation of crustal material[26,28,29,40,41]. The decoupling of MIF-S from REE and Os isotope systematics in Y98 therefore suggests that the relationship between MIF-S anomalies and crustal assimilation may not be universal among Martian meteorites and implies that additional processes may have contributed to the incorporation of anomalous sulfur in Y98. Instead, it is possible that either (1) the MIF-S reflected by late-stage sulfides was already present in the parental melt or source (i.e., inherited from a mantle reservoir), or (2) sulfur and incompatible element systematics were decoupled during the process that introduced MIF-S (e.g., sulfide-silicate partitioning or metasomatic addition of sulfide-rich, REE-poor material; refer section 4.3.1 for detailed information).

Gadamis 001, by contrast, shows large $\Delta^{33}S$ variability without obvious late-stage textures. Although Gadamis 001 is compositionally enriched, this does not necessarily imply a crustal sulfur origin; the sulfides may instead record inheritance from a mantle source already bearing MIF-S signatures. Thus, crustal assimilation may explain a subset of observations (especially in meteorites with clear alteration or sulfates), but it cannot account for the full spectrum of $\Delta^{33}S$ behaviour in shergottites. Note, that within a small magmatic reservoir, it is expected that the sulfur isotope composition will be homogenized. Thus, the data presented here raises a "scale" issue with respect to a single hand sample (specifically in Gadamis 001) that is difficult to reconcile. We thus consider the possible role of additional, previously unexplored processes that may act independent of the size of the melt reservoir, in establishing the MIF-S signatures preserved in Martian mantle reservoirs.

Inheriting sulfur isotope heterogeneity from the Solar Nebula

One possible explanation for the observed $\Delta^{33}S$ heterogeneity is that the Martian mantle was originally isotopically heterogeneous. Such heterogeneity could reflect MIF-S signatures inherited directly from the solar nebula. However, scenarios invoking MIF-S inheritance from the solar nebula are inconsistent with current geochemical and isotopic constraints. The Sm-Nd, Rb-Sr, and Hf-W isotope systematics of shergottites indicate that their source reservoirs differentiated shortly after magma ocean crystallisation (~4.5 Ga) and have remained largely isolated since[42,43]. Available bulk $\Delta^{33}S$ data from meteorites sampling early formed planetesimals show small MIF-S signatures likely inherited from the solar nebula; however, these anomalies are multiple orders of magnitude smaller [5,6,35]. Therefore, the relatively large MIF-S anomalies observed in this study are unlikely to reflect a nebular origin.

Contributions from Carbonaceous Chondrite-Like Materials

Carbonaceous chondrite-like materials can carry small but measurable $\Delta^{33}S$ anomalies among individual sulfur-bearing phases (e.g., FeS versus S^0) and could, in principle, have delivered sulfur to the Martian surface during the initial or possible late accretion history. However, the bulk $\Delta^{33}S$ values of chondrites remain close to 0.00‰ [4]. Consequently, the addition of such material would primarily affect sulfur concentrations rather than isotopic compositions. Moreover, the magnitude and pattern of isotopic heterogeneity observed in our dataset cannot be reconciled with contributions from any known chondritic group[4,5]. The long-term isotopic isolation of shergottite mantle sources and the lack of correlation between $\Delta^{33}S$ and siderophile element abundances further argue against late-stage meteoritic overprinting[44]. While small contributions from an unidentified external sulfur reservoir cannot be entirely excluded, stochastic late accretion events cannot explain the systematic $\Delta^{33}S$ differences between distinct shergottite groups.

An Early-Formed Martian MIF-S Reservoir

Given the available constraints, the most plausible explanation involves the existence of an early-formed MIF-S reservoir within the Martian mantle. To explain the data, we hypothesise that the early-formed MIF-S reservoir likely originated through large-scale atmosphere-mantle exchange during or shortly after magma ocean crystallisation. Extensive degassing and volatile recycling could have enabled isotopically anomalous sulfur, produced by early gas-phase photochemistry, to be incorporated into the solidifying mantle. Subsequent partial melting and redox-controlled sulfur partitioning could then have preserved and expressed these ancient signatures in the parental magmas of shergottites. The following sections explore the feasibility of an early-formed MIF-S reservoir in the martian mantle in more detail.

Was there an early formed MIF-S reservoir in the Martian Mantle?

If the observed MIF-S was inherited from an early-formed mantle reservoir, the mechanism responsible for transporting the MIF-S-bearing reservoir into the Martian mantle remains unknown. One possibility is that MIF-S was introduced to the Martian mantle through processes involving early mantle-atmosphere exchange, beginning during magma ocean crystallisation and continuing through the generation of later-stage melts. Such may be achieved by crustal delamination or ingassing of photolytic sulfur during magma ocean crystallisation. Notably, we cannot unambiguously discriminate constrain the exact pathway (or combination of pathways) of mantle-atmosphere exchange and a single mechanism of mantle-atmosphere exchange recorded by all samples is not necessary. We use the term “exchange” in a general sense, as the dominant pathway may have changed through time and could include ingassing during magma ocean

crystallisation, recycling of crustal sulfur via delamination, and/or crustal assimilation during magma generation. For the purposes of this study, we treat them as equally viable.

Crustal delamination as a mechanism to transport MIF-S reservoir in the Martian Mantle

Mars' relatively thin crust [45] possibly allowed MIF-S reservoirs to accumulate at the surface early in the planet's history. Subsequent volcanic activity could have buried these sulfur-enriched layers beneath basaltic flows, gradually driving them deeper into the crust [45]. Later episodes of crustal delamination, possibly driven by mantle plume activity, may have facilitated the downward transport of these surface-derived materials into the mantle [46]. Martian mantle plumes could have induced significant melting in the Martian mantle, evidenced by regions like Tharsis, which is characterized by extensive volcanic activity and topographical anomalies [46]. The formation of volcanic provinces such as Tharsis and Elysium, potentially led to partial melting of the crust and the entrainment of surface materials into rising magmas [46]. However, if plume-driven magmatism weakened the lithosphere, it could have caused simultaneous detachment and sinking of the lower crust, carrying surface-derived material downward [47].

An alternative hypothesis draws parallels with Archean Earth, suggesting that Mars may have experienced a form of lithospheric recycling known as "dripping tectonics". Unlike modern plate tectonics, this process involves the viscous deformation of the lithosphere driven by high-temperature mantle convection, where dense lower lithospheric materials sink into the underlying asthenosphere in a manner reminiscent of falling droplets [48–50]. On Mars, such gravitational instabilities could have developed in areas of the lithosphere where dense mafic cumulates or eclogitized crustal materials accumulated, leading to localized drips that transported these

components into the deeper mantle [51]. As these drips descended, they would have induced upwelling and decompression melting in the surrounding mantle, potentially remelting dripped crustal material and producing magmas with recycled signatures. Support for this process exists in seismic data from the InSight mission, which suggest the Martian mantle has a complex and heterogeneous lithosphere with zones of partial melt, that may be a relic of lithospheric dripping or delamination processes [52]. Crustal delamination offers a plausible explanation for the coexistence of depleted and enriched shergottites, as well as the presence of evolved igneous rocks observed both from orbit and in situ [53–55]. While not equivalent to Earth's plate tectonics, dripping tectonics provides a viable framework for the deep transport and recycling of crustal materials on Mars, potentially explaining geochemical features such as MIF-S incorporation into the mantle.

If processes like crust delamination transported crustal material containing MIF-S into the deep mantle, it is plausible that REE enriched crustal components could also have been carried along with the crustal materials. This prompts the question of why REE enrichment is absent in some shergottites. This lack of REE enrichment in depleted shergottites with MIF-S anomalies can be resolved by interpreting MIF-S signal as originating from pre-differentiated mantle reservoirs established during magma ocean solidification at ~4.52 Ga, consistent with the shergottite isotopic framework. In this scenario, incompatible-element-depleted and enriched mantle domains formed early and remained largely isolated until later melting events that produced the shergottites. The observed REE-MIF decoupling therefore reflects phase-specific partitioning and redox-controlled melting within these long-lived reservoirs rather than repeated large-scale re-melting of crustal material. Under the moderately reducing conditions typical of depleted shergottite sources (ΔFMQ -2 to -3), sulfides behave as a refractory phase that remains in the residue once silicate melt extraction begins[37,56,57]. This allows REE-enriched silicate melts to be extracted while MIF-S

bearing sulfur remains sequestered in residual sulfides. A subsequent small degree melting, or metasomatic event could later release this isotopically anomalous sulfur into a melt that is otherwise depleted in incompatible elements.

Importantly, variations in oxygen fugacity between shergottite groups (IW to FMQ [58,59]) likely modulate this behaviour. More oxidized (enriched) magmas would promote sulfur mobilization and isotopic homogenisation, whereas reduced (depleted) magmas could preserve MIF-S heterogeneity. This relationship may also link to observed chlorine isotope differences between the two groups[60,61], suggesting variable volatile recycling or crustal interaction under distinct redox regimes.

In-gassing of Photolytic Sulfur During Magma Ocean Crystallisation

The large variability in $\delta^{34}S$ values and the systematic evolution from depleted to enriched shergottites provide key insights into how mass-independent sulfur isotope anomalies (MIF-S) were incorporated into the Martian mantle. The magma ocean isotopic fractionation-mixing model proposed here, analogous to an assimilation-fractional crystallisation (AFC) framework, can also account for the observed MIF-S variability in the studied shergottites. As shown earlier, the magma ocean crystallisation part of this model predicts that $\delta^{34}S$ evolved from approximately −1.5‰ to +1‰ during magma ocean crystallisation, consistent with the transition from depleted to enriched mantle reservoirs.

The incorporation of MIF-S into the Martian mantle could have occurred during the crystallisation of an early global magma ocean. In this scenario, photolytic sulfur, carrying $\Delta^{33}S$ anomalies, would have been present in the primordial Martian atmosphere. As the magma ocean cooled and began

to crystallize, it would have continued to interact with the overlying atmosphere, creating conditions favourable for volatile in-gassing (Fig. 5a). Volatile in-gassing occurs as atmospheric species dissolve back into the silicate melt. If the magma ocean remained in contact with the photochemically altered atmosphere during its crystallisation, MIF-S-bearing sulfur could have been sequestered into the interior. The extent of sulfur incorporation depends on variable parameters such as gas solubility, melt composition, pressure, and temperature, ultimately resulting in spatially heterogeneous reservoirs within the mantle carrying MIF-S signatures. This process would have been particularly efficient during periods of surface cooling, when in-gassing rates could exceed outgassing rates. Ingassing during magma ocean crystallisation offers a plausible pathway for the early introduction of MIF-S into the Martian interior before final crystallisation of the mantle and thereby preserving atmospherically processed sulfur in primitive shergottite source regions.

Ultimately the process of in-gassing of photochemically processed sulfur during magma ocean crystallisation offers a coherent framework that simultaneously explains both the $\Delta^{33}S$ and $\delta^{34}S$ variability. Our isotopic fractionation-mixing model[62], shows that a combination of early in-gassing of MIF-S and isotopic fractionation during sulfide saturation can reproduce the full range of sulfur isotope compositions observed in the shergottites (Fig. 5). These results indicate that the sulfur isotope systematics of Martian meteorites can be explained without invoking late-stage crustal assimilation (cf. [63]). Instead, regional mantle heterogeneities in both $\delta^{34}S$ and $\Delta^{33}S$ could reflect primary features established during early atmosphere-mantle interaction. The survival of such heterogeneities suggests limited mantle homogenization and underscores the importance of early global-scale processes in shaping Mars' volatile inventory.

Implications for sulfur delivery to the terrestrial planets

Our observations provide a potential explanation for the sulfur isotope anomalies reported in other planetary materials. The presence of $\Delta^{33}S$ heterogeneity in Martian shergottites is consistent with signatures preserved in Howardite-Eucrite-Diogenite, iron, and pallasite meteorites [1,3,16] , and Apollo 17 lunar pyroclastic orange glass beads [64]. Unlike Earth, where convective mixing and plate tectonics likely erased comparable signatures, Mars and smaller bodies that lacked extensive mantle mixing can retain isotopic evidence of atmosphere-mantle interactions. The absence of such anomalies among samples that derive from Earth's mantle does not preclude their existence. Instead identifying such exotic components may require targeted analyses of ancient, potentially undegassed, mantle and core domains. At present, it remains unclear whether the processes we invoke, such as early crustal delamination and/or sulfur in-gassing during magma ocean crystallisation, mask or overprint any primordial isotopic signatures tied to the precursors responsible for the delivery of sulfur to the Earth. As such, efforts to directly trace the origin of planetary sulfur inventories, is likely littered with more complication than previously assumed. To properly constrain the genetic origin of sulfur across solar system bodies, detailed geochemical and seismic (for the Earth) constraints are necessary.

Conclusion

The sulfur isotope variability reported in this study, as well as among previous work, underscores the dynamic interplay of volatiles among the Martian interior, surface, and atmosphere [22–26,28,39]. The presence of anomalous $\Delta^{33}S$ values in these four shergottites raises important questions about the mechanisms responsible for sulfur isotope variations in Martian meteorites. While previous studies have attributed anomalous $\Delta^{33}S$ values in nakhlites and chassignites to crustal assimilation,

the analysed shergottites do not show clear correlations between $\Delta^{33}S$ and key indicators of crustal assimilation (e.g.,$^{187}Os/^{188}Os$ or $^{206}Pb/^{204}Pb$.), thereby necessitating an alternative explanation. Overall, these findings indicate that sulfur isotope systematics in shergottites cannot be solely explained by crustal assimilation, as seen in nakhlites. A compelling possibility involved the incorporation of photolytic sulfur addition during the crystallisation of the Martian magma ocean, may best explain the $\Delta^{33}S$ anomalies seen across the full compositional spectrum of shergottites. While deep transport of atmospherically processed sulfur is probable, it raises key questions regarding the transport mechanisms in the absence of plate tectonics, which currently is poorly constrained. Although bulk analyses of shergottites show $\Delta^{33}S$ and $\delta^{34}S$ values close to 0.00‰ with no correlations to other isotope systems, in situ SIMS analysis reveals anomalous $\Delta^{33}S$, emphasizing the need for further in situ investigations to identify the possibly distinct sulfur components trapped among olivine and pyroxene phenocrysts. Future research integrating high-precision isotope measurements, experimental studies, and comprehensive geochemical analyses will be essential to refine our understanding of Martian sulfur cycling and mantle-crust interactions.

Materials and Methods

Electron Microprobe Analysis

Electron Microprobe Analysis (EMPA) was conducted at the Massachusetts Institute of Technology's (MIT) Electron Microprobe Facility using the JEOL JXA-8200. The instrument was operated under conditions set at a 15 kV accelerating voltage and a 10nA beam current. Quantitative analysis was performed using wavelength dispersive spectrometry (WDS) with a

counting time of 40 seconds per element. Standards used for calibration included $CuFeS_2$ for Cu, FeS for Fe and S, NiS for Ni, ZnS for Zn, and TiO_2 for Ti. For spatial analysis, Ti, Si, S, Fe, and Al were mapped using WDS, while Mg, Ca, and Cr were mapped with an energy dispersive spectrometer (EDS). The maps were captured at a resolution of 1024 x 1024 pixels, with a dwell time of 20 milliseconds per pixel. Spatial resolution was 10 microns per pixel for Tissint and Y98, and 12 microns per pixel for Gadamis 001 and NWA 11300. Data were collected in stage-raster mode, where the beam remains stationary, and the stage moves beneath it. The analysis totals for Gadamis appear slightly high (i.e., > 100%; Table 1), potentially due to factors such as charging or surface roughness. However, calibration is confirmed to be accurate, as the other samples exhibited total mass percentages of 100%.

Synthesis of troilite standard for Secondary Ion Mass Spectrometry

To analyse the sulfides with elemental compositions like that of a troilite, we synthesised a troilite standard using a starting material that consisted of high-purity iron sulfide (FeS) powder (99.99 wt.%). Synthesis was conducted at Brown University using a salt-Pyrex® sleeve, a straight-walled graphite furnace, and an internal crushable MgO spacer housed within a graphite-lined molybdenum capsule. The graphite capsule featured a central cavity measuring 7 mm in length and 3 mm in diameter. This configuration enabled the capsule to be sectioned transversely at its midpoint following the experiment, with one half allocated for bulk sulfur isotope analysis and the other for Secondary Ion Mass Spectrometry (SIMS). Following assembly, the experimental setup was loaded into a piston-cylinder apparatus and pressurized to slightly above the target pressure of 0.5 GPa. The temperature was then increased at a controlled rate of 75 °C/min to a value 50–100 °C above the estimated liquidus temperature of the starting material (~1250 °C; *56*). Once both

the target pressure and temperature were attained, the system was held under these conditions for one hour to ensure melt homogeneity. To suppress crystal growth and inhibit the formation of basal fractures, the sample was subsequently step-quenched to 600 °C. Upon completion of the run, the molybdenum capsule was sectioned, embedded in epoxy, and polished for subsequent analytical work. Backscattered electron images and Electron Microprobe analysis results of the synthesized troilite (FeS) standard are provided in Supplementary Tables S1and S2 and Supplementary Figure S16.

Bulk sulfur isotope analysis

Wet chemistry

To verify that sulfur in synthesised FeS did not undergo isotopic fractionation during the experimental procedures, we conducted sulfur isotope analyses on both the starting material used to synthesize the standard and the troilite standard recovered after the experiment. Pre- and post-experiment materials were reacted converted to Ag_2S closely following procedures outlined in [66], using a modified Teflon-only set-up [67,68]. 20 ml of 5N hydrochloric acid (HCl) was injected into an N_2 purged Teflon digestion vessel that is connected, first, to a water trap, followed by a silver nitrate–nitric acid capture solution trap. Under a continuous flow of N_2, the FeS was allowed to react with the HCl at ~ 70 °C for 2.5 hours. Such a reaction yields H_2S, which was first bubbled through a water trap to capture an HCl vapours, and ultimately converted to Ag_2S when bubbled through the capture solution [67]. After the reaction was complete, the Ag_2S was extracted by centrifugation and decantation of the $AgNO_3$ supernatant, transferred to 1.5ml Eppendorf centrifuge vessels and cleaned 6 times with Milli-Q water. After removing most of the supernatant with a transfer pipette, the Ag_2S was dried at 70°C in preparation for conversion to SF_6.

Fluorination

Samples were fluorinated and analysed for S isotopes at the MIT. Provided as Ag_2S were pre-weighed into solvent-cleaned aluminium foil and fluorinated under a ~100 torr fluorine atmosphere at 300 °C overnight. This reaction converted silver-bound sulfur into SF_6 gas. The resultant SF_6 was purified using a custom-built, fully automated cryogenic preparative gas chromatography system. Quadruple sulfur isotope analysis of the purified SF_6 was performed using a ThermoScientific™ MAT 253 isotope ratio mass spectrometer equipped with a multiport system, monitoring SF_5^+ ion beams at mass-to-charge (m/z) ratios of 127, 128, 129, and 131. For traceability and standardization, ~3 mg aliquots of IAEA-S1, S2, and S3 sulfur isotope standards were processed alongside unknown samples (Table S1). A regression of the IAEA standards was used to normalize $\delta^{34}S$ data to the Vienna Canyon Diablo Troilite (VCDT) scale. The sulfur isotopic compositions of the synthesized standards are provided in Supplementary Table S3.

Secondary Ion Mass Spectrometry

Secondary Ion Mass Spectrometry (SIMS) analyses were performed using the Cameca IMS 1280 at the Northeast National Ion Microprobe Facility (NENIMF) at the Woods Hole Oceanographic Institution (WHOI). A $^{133}Cs^+$ primary ion beam with a current of 350 pA was accelerated to 10 kV and focused to a spot diameter of approximately 5 µm. A 5 x 5 µm raster was applied, resulting in a final crater diameter of about 10 µm at its longest dimension. Secondary ions of ^{32}S-, ^{33}S-, and ^{34}S- were sputtered and then accelerated at 10 kV, magnified 80X, and directed through a 400 µm diameter contrast aperture, a 101 µm entrance slit, a 1500 x 1500 µm square field aperture, and a 50 eV energy window. The ions were detected in multicollection mode. The secondary magnet was calibrated to axial mass 33.47 and stabilized using an NMR probe. The ^{32}S- ion was counted

using a 10^{11} Ω Faraday cup at L1, $^{33}S^-$ was measured with a Hamamatsu electron multiplier at C, and $^{34}S^-$ ions were detected with a 10^{11} Ω Faraday cup at H1. Slits with a width of 250 µm were placed before each detector to achieve a mass resolving power of 4998 (~5000), which is sufficient to resolve sulfur ion masses from any hydride or oxide isobars (e.g., $^{31}P^1H$, $^{32}S^1H$, $^{33}S^1H$, $^{16}O_2$, $^{16}O^{17}O$, $^{17}O_2$).

SIMS data reduction

We collected sulfur isotope data on unknown sulfide grains over a period of four days, with an additional fifth day at the beginning of the session dedicated to analysing pyrrhotite, troilite, and pentlandite standards. The following standards were used to calibrate the instrument settings and evaluate instrumental fractionation caused by different ionisation efficiencies of sulfides with different compositions: Anderson Pyrrhotite[69], AMNH 112266, synthetic Troilite standard (recorded as Lab_Std, synthesized at Brown), Nifty [70], Crystal_Sierra [70], and AMNH 26170 (Table 3).

To correct for instrumental mass fractionation, we used the in-house pyrrhotite (112266_Po) and troilite (Lab_Std) standards respectively, as additional bracketing standards during the analyses, with an almost perfect matrix match. The standards were placed on a separate indium mound. For bracketing, an average of three measurements of 112266_Po and Lab_Std each were performed, which were then used to bracket and correct for instrumental drift. For data reduction, raw ratios of $^{33}S/^{32}S$ and $^{34}S/^{32}S$ from Y98, Tissint, and NWA 11300 were normalized to the average $^{33}S/^{32}S$ and $^{34}S/^{32}S$ ratios of 112266_Po, as these meteorites have sulfides of pyrrhotite compositions. Sulfides in Gadamis 001 are troilites thus raw ratios from Gadamis 001 were normalized to the average $^{33}S/^{32}S$ and $^{34}S/^{32}S$ ratios of Lab_Std. The $^{34}S/^{32}S$ values were then renormalized to the

published values of V-CDT from [71] and $^{33}S/^{32}S$ was renormalized to the measured value of CDT reported in [1]. The sulfur isotope data is reported in per mil (‰) using the following formulas:

$$\delta^{33}S = \left[\left(\frac{(^{33}S/^{32}S)_{sample}}{(^{33}S/^{32}S)_{CDT}}\right) - 1\right] \times 1000 \quad (1)$$

$$\delta^{34}S = \left[\left(\frac{(^{34}S/^{32}S)_{sample}}{(^{34}S/^{32}S)_{V-CDT}}\right) - 1\right] \times 1000 \quad (2)$$

$$\Delta^{33}S = \delta^{33}S - 1000((\left(\frac{\delta^{34}S}{1000}\right) + 1)^{0.515} - 1) \quad (3)$$

For determining the uncertainty of the δ values of the standards, we applied the following equations:

- For Y98, Tissint, and NWA11300 with respect to 112266_Po:
  - $1\sigma_{34}R = 1000 \times$

$$\sqrt{((\sigma_{34}R_{sample\_raw})^2 \times (^{34}R_{avg\_112266})^{-2}) + ((^{34}R_{sample\_raw})^2 \times (1\sigma_{34}R_{112266})^2 \times (^{34}R_{avg\_112266})^{-4})} \quad (4)$$

  - $1\sigma_{33}R = 1000 \times$

$$\sqrt{((\sigma_{33}R_{sample\_raw})^2 \times (^{33}R_{avg\_112266})^{-2}) + ((^{33}R_{sample\_raw})^2 \times (1\sigma_{33}R_{112266})^2 \times (^{34}R_{avg\_112266})^{-4})} \quad (5)$$

- For Gadamis 001 with respect to Lab_Std:
  - $1\sigma_{34}R = 1000 \times$

$$\sqrt{((\sigma_{34}R_{sample\_raw})^2 \times (^{34}R_{avg\_Lab\_STD})^{-2}) + ((^{34}R_{sample\_raw})^2 \times (1\sigma_{34}R_{avg\_Lab\_STD})^2 \times (^{34}R_{avg\_Lab\_STD})^{-4})} \quad (6)$$

- $1\sigma_{33}R = 1000 \times$

$$\sqrt{((\sigma_{33}R_{sample\_raw})^2 \times ({}^{33}R_{avg\_Lab\_STD})^{-2}) + ((\,{}^{33}R_{sample\_raw})^2 \times (1\sigma_{33}R_{avg\_Lab\_STD})^2 \times ({}^{34}R_{avg\_Lab\_STD})^{-4})} \quad (7)$$

For $\Delta^{33}S$ values, we report our uncertainties not assuming co-variance of $\delta^{33}S$ and $\delta^{34}S$. The $2\boldsymbol{\sigma}$ uncertainty on individual measurements of $\delta^{33}S$, $\delta^{34}S$ and $\Delta^{33}S$ on all standards ranges from 0.06 ‰ to 0.26 ‰, 0.28 ‰ to 0.56 ‰, and 0.30‰ to 0.56‰ respectively. Using this outlined normalization scheme and error propagation, we find that our analyses of standards are consistent with typical high-temperature mass-dependent fractionation of sulfur, plotting within error of a slope of 0.515 on a plot of $\delta^{33}S$ vs. $\delta^{34}S$ (Supplementary Figure. S2), with similar reproducibility to that published on using similar analytical protocols (e.g.,[72]. Our measurement of Lab_Std yielded an average $\Delta^{33}S$ value of 0.0426± 0.43 (2 S.D.) and 112266_Po an average $\Delta^{33}S$ value of 0.085 ± 0.41 (2 S.D.), which is consistent with values obtained for Lab_Std ($\Delta^{33}S$ = 0.036 ± 0.014, 2 S.D.) and Po_112266 ($\Delta^{33}S$ = 0.077 ± 0.003, 2 S.E.) using bulk techniques, demonstrating our ability to resolve mass-independent signatures among mass-dependent standards. Details of the SIMS analyses are provided in the Supplementary Dataset S1, Dataset S4.

References

1. Antonelli, M. A. *et al.* Early inner solar system origin for anomalous sulfur isotopes in differentiated protoplanets. *Proceedings of the National Academy of Sciences* **111**, 17749–17754 (2014).
2. Chakraborty, S., Jackson, T. L., Ahmed, M. & Thiemens, M. H. Sulfur isotopic fractionation in vacuum UV photodissociation of hydrogen sulfide and its potential relevance to meteorite analysis. *Proceedings of the National Academy of Sciences of the United States of America* **110**, 17650–17655 (2013).
3. Rai, V. K., Jackson, T. L. & Thiemens, M. H. Photochemical Mass-Independent Sulfur Isotopes in Achondritic Meteorites. *Science* **309**, 1062–1065 (2005).
4. Labidi, J., Farquhar, J., Alexander, C. M. O., Eldridge, D. L. & Oduro, H. Mass independent sulfur isotope signatures in CMs: Implications for sulfur chemistry in the early solar system. *Geochimica et Cosmochimica Acta* **196**, 326–350 (2017).
5. Bullock, E. S., McKEEGAN, K. D., Gounelle, M., Grady, M. M. & Russell, S. S. Sulfur isotopic composition of Fe-Ni sulfide grains in CI and CM carbonaceous chondrites. *Meteoritics & Planetary Science* **45**, 885–898 (2010).
6. Rai, V. K. & Thiemens, M. H. Mass independently fractionated sulfur components in chondrites. *Geochimica et Cosmochimica Acta* **71**, 1341–1354 (2007).
7. Elkins-Tanton, L. T. Linked magma ocean solidification and atmospheric growth for Earth and Mars. *Earth and Planetary Science Letters* **271**, 181–191 (2008).
8. Elkins-Tanton, L. T. Magma Oceans in the Inner Solar System. *Annual Review of Earth and Planetary Sciences* **40**, 113–139 (2012).

9. Young, E. D., Shahar, A. & Schlichting, H. E. Earth shaped by primordial H2 atmospheres. *Nature* **616**, 306–311 (2023).
10. Mundl-Petermeier, A. *et al.* Anomalous 182W in high 3He/4He ocean island basalts: Fingerprints of Earth's core? *Geochimica et Cosmochimica Acta* **271**, 194–211 (2020).
11. Messling, N. *et al.* Ru and W isotope systematics in ocean island basalts reveals core leakage. *Nature* 1–5 (2025) doi:10.1038/s41586-025-09003-0.
12. Horton, F. *et al.* Highest terrestrial 3He/4He credibly from the core. *Nature* **623**, 90–94 (2023).
13. Labidi, J. *et al.* Experimentally determined sulfur isotope fractionation between metal and silicate and implications for planetary differentiation. *Geochimica et Cosmochimica Acta* **175**, 181–194 (2016).
14. Labidi, J. & Cartigny, P. Negligible sulfur isotope fractionation during partial melting: Evidence from Garrett transform fault basalts, implications for the late-veneer and the hadean matte. *Earth and Planetary Science Letters* **451**, 196–207 (2016).
15. Wang, W. *et al.* Sulfur isotopic signature of Earth established by planetesimal volatile evaporation. *Nat. Geosci.* **14**, 806–811 (2021).
16. Dottin, J. W., Farquhar, J. & Labidi, J. Multiple sulfur isotopic composition of main group pallasites support genetic links to IIIAB iron meteorites. *Geochimica et Cosmochimica Acta* **224**, 276–281 (2018).
17. Ranta, E. *et al.* Ancient and recycled sulfur sampled by the Iceland mantle plume. *Earth and Planetary Science Letters* **584**, 117452–117452 (2022).
18. Franz, H. B. *et al.* Isotopic links between atmospheric chemistry and the deep sulphur cycle on Mars. *Nature* **508**, 364–368 (2014).

19. Udry, A. *et al.* What Martian Meteorites Reveal About the Interior and Surface of Mars. *Journal of Geophysical Research: Planets* **125**, e2020JE006523 (2020).

20. Farquhar, J., Savarino, J., Jackson, T. L. & Thiemens, M. H. Evidence of atmospheric sulphur in the martian regolith from sulphur isotopes in meteorites. *Nature* **404**, 50–52 (2000).

21. Franz, H. B. *et al.* LARGE SULFUR ISOTOPIC ANOMALIES IN SHERGOTTITES GADAMIS 001 AND NORTHEAST. (2021).

22. Franz, H. B., Wu, N., Farquhar, J. & Irving, A. J. A new type of isotopic anomaly in shergottite sulfides. *Meteoritics & Planetary Science* **54**, 3036–3051 (2019).

23. Dottin, J. W. *et al.* Evidence for oxidation at the base of the nakhlite pile by reduction of sulfate salts at the time of lava emplacement. *Geochimica et Cosmochimica Acta* **239**, 186–197 (2018).

24. Farquhar, J., Kim, S.-T. & Masterson, A. Implications from sulfur isotopes of the Nakhla meteorite for the origin of sulfate on Mars. *Earth and Planetary Science Letters* **264**, 1–8 (2007).

25. Lorand, J.-P. *et al.* The sulfur budget and sulfur isotopic composition of Martian regolith breccia NWA 7533. *Meteoritics & Planetary Science* **55**, 2097–2116 (2020).

26. Day, J. M. D., Paquet, M., Udry, A. & Moynier, F. A heterogeneous mantle and crustal structure formed during the early differentiation of Mars. *Science Advances* **10**, eadn9830 (2024).

27. Brounce, M., Boyce, J. W. & McCubbin, F. M. Sulfur in apatite from the Nakhla meteorite record a late-stage oxidation event. *Earth and Planetary Science Letters* **595**, 117784 (2022).

28. Mari, N. *et al.* Syneruptive incorporation of martian surface sulphur in the nakhlite lava flows revealed by S and Os isotopes and highly siderophile elements: implication for mantle sources in Mars. *Geochimica et Cosmochimica Acta* **266**, 416–434 (2019).

29. Usui, T., McSween, H. Y. & Floss, C. Petrogenesis of olivine-phyric shergottite Yamato 980459, revisited. *Geochimica et Cosmochimica Acta* **72**, 1711–1730 (2008).

30. Mikouchi, T. *et al.* Yamato 980459: Mineralogy and petrology of a new shergottite-related rock from Antarctica. *Antarctic Meteorite Research* **17**, 13 (2004).

31. Balta, J. B., Sanborn, M. E., Udry, A., Wadhwa, M. & McSween Jr., H. Y. Petrology and trace element geochemistry of Tissint, the newest shergottite fall. *Meteoritics & Planetary Science* **50**, 63–85 (2015).

32. Liu, Y., Baziotis, I. P., Asimow, P. D., Bodnar, R. J. & Taylor, L. A. Mineral chemistry of the Tissint meteorite: Indications of two-stage crystallization in a closed system. *Meteoritics & Planetary Science* **51**, 2293–2315 (2016).

33. Saal, A. E. & Hauri, E. H. Large sulfur isotope fractionation in lunar volcanic glasses reveals the magmatic differentiation and degassing of the Moon. *Science Advances* **7**, eabe4641 (2021).

34. von Gehlen, K. Sulfur in the Earth's Mantle — A Review. in *Early Organic Evolution: Implications for Mineral and Energy Resources* (eds Schidlowski, M., Golubic, S., Kimberley, M. M., McKirdy, D. M. & Trudinger, P. A.) 359–366 (Springer Berlin Heidelberg, Berlin, Heidelberg, 1992). doi:10.1007/978-3-642-76884-2_27.

35. Labidi, J., Cartigny, P. & Moreira, M. Non-chondritic sulphur isotope composition of the terrestrial mantle. *Nature* **501**, 208–211 (2013).

36. Gaillard, F., Scaillet, B. & Arndt, N. T. Atmospheric oxygenation caused by a change in volcanic degassing pressure. *Nature* **478**, 229–232 (2011).

37. Gaillard, F. & Scaillet, B. A theoretical framework for volcanic degassing chemistry in a comparative planetology perspective and implications for planetary atmospheres. *Earth and Planetary Science Letters* **403**, 307–316 (2014).

38. Wing, B. A. & Farquhar, J. Sulfur isotope homogeneity of lunar mare basalts. *Geochimica et Cosmochimica Acta* **170**, 266–280 (2015).

39. Greenwood, J. P., Riciputi, L. R., McSween, H. Y. & Taylor, L. A. Modified sulfur isotopic compositions of sulfides in the nakhlites and Chassigny. *Geochimica et Cosmochimica Acta* **64**, 1121–1131 (2000).

40. Shearer, C. K. *et al.* Petrogenetic linkages among Martian basalts: Implications based on trace element chemistry of olivine. *Meteoritics & Planetary Science* **43**, 1241–1258 (2008).

41. Peters, T. J. *et al.* Tracking the source of the enriched martian meteorites in olivine-hosted melt inclusions of two depleted shergottites, Yamato 980459 and Tissint. *Earth and Planetary Science Letters* **418**, 91–102 (2015).

42. Borg, L. E., Brennecka, G. A. & Symes, S. J. K. Accretion timescale and impact history of Mars deduced from the isotopic systematics of martian meteorites. *Geochimica et Cosmochimica Acta* **175**, 150–167 (2016).

43. Debaille, V., Yin, Q.-Z., Brandon, A. D. & Jacobsen, B. Martian mantle mineralogy investigated by the 176Lu–176Hf and 147Sm–143Nd systematics of shergottites. *Earth and Planetary Science Letters* **269**, 186–199 (2008).

44. Foley, C. N. *et al.* The early differentiation history of Mars from 182W-142Nd isotope systematics in the SNC meteorites. *Geochimica et Cosmochimica Acta* **69**, 4557–4571 (2005).

45. Nimmo, F. & Tanaka, K. EARLY CRUSTAL EVOLUTION OF MARS1. *Annual Review of Earth and Planetary Sciences* **33**, 133–161 (2005).

46. Reese, C. C., Solomatov, V. S., Baumgardner, J. R., Stegman, D. R. & Vezolainen, A. V. Magmatic evolution of impact-induced Martian mantle plumes and the origin of Tharsis. *Journal of Geophysical Research: Planets* **109**, (2004).

47. Gleeson, M. Plume-induced subduction. *Nat Rev Earth Environ* **1**, 139–139 (2020).

48. Cawood, P. A. *et al.* Geological archive of the onset of plate tectonics. *Philosophical Transactions of the Royal Society A: Mathematical, Physical and Engineering Sciences* **376**, 20170405 (2018).

49. Lenardic, A. The diversity of tectonic modes and thoughts about transitions between them. *Philosophical Transactions of the Royal Society A: Mathematical, Physical and Engineering Sciences* **376**, 20170416 (2018).

50. Liu, S. *et al.* Archean crust-mantle geodynamic regimes: A review. *Geosystems and Geoenvironment* **1**, 100063 (2022).

51. Rozel, A., Golabek, G. J., Näf, R. & Tackley, P. J. Formation of ridges in a stable lithosphere in mantle convection models with a viscoplastic rheology. *Geophysical Research Letters* **42**, 4770–4777 (2015).

52. Knapmeyer-Endrun, B. *et al.* Thickness and structure of the martian crust from InSight seismic data. *Science* **373**, 438–443 (2021).

53. Carter, J. & Poulet, F. Ancient plutonic processes on Mars inferred from the detection of possible anorthositic terrains. *Nature Geosci* **6**, 1008–1012 (2013).

54. McSween, H. Y., Taylor, G. J. & Wyatt, M. B. Elemental Composition of the Martian Crust. *Science* **324**, 736–739 (2009).

55. Sautter, V. *et al.* In situ evidence for continental crust on early Mars. *Nature Geosci* **8**, 605–609 (2015).

56. Gaillard, F. & Scaillet, B. The sulfur content of volcanic gases on Mars. *Earth and Planetary Science Letters* **279**, 34–43 (2009).

57. Ding, S., Dasgupta, R., Lee, C.-T. A. & Wadhwa, M. New bulk sulfur measurements of Martian meteorites and modeling the fate of sulfur during melting and crystallization – Implications for sulfur transfer from Martian mantle to crust–atmosphere system. *Earth and Planetary Science Letters* **409**, 157–167 (2015).

58. Herd, C. D. K., Borg, L. E., Jones, J. H. & Papike, J. J. Oxygen fugacity and geochemical variations in the martian basalts: implications for martian basalt petrogenesis and the oxidation state of the upper mantle of Mars. *Geochimica et Cosmochimica Acta* **66**, 2025–2036 (2002).

59. Herd, C. D. K. The oxygen fugacity of olivine-phyric martian basalts and the components within the mantle and crust of Mars. *Meteoritics & Planetary Science* **38**, 1793–1805 (2003).

60. Sharp, Z., Williams, J., Shearer, C., Agee, C. & McKeegan, K. The chlorine isotope composition of Martian meteorites 2. Implications for the early solar system and the formation of Mars. *Meteoritics & Planetary Science* **51**, 2111–2126 (2016).

61. Shearer, C. K. *et al.* Distinct chlorine isotopic reservoirs on Mars. Implications for character, extent and relative timing of crustal interactions with mantle-derived magmas, evolution of

the martian atmosphere, and the building blocks of an early Mars. *Geochimica et Cosmochimica Acta* **234**, 24–36 (2018).

62. DePaolo, D. J. Trace element and isotopic effects of combined wallrock assimilation and fractional crystallization. *Earth and Planetary Science Letters* **53**, 189–202 (1981).
63. Udry, A., Ostwald, A. M., Day, J. M. D. & Hallis, L. J. Fundamental constraints and questions from the study of Martian meteorites and the need for returned samples. *Proceedings of the National Academy of Sciences* **122**, e2404254121 (2025).
64. Dottin III, J. W., Kim, S.-T., Wing, B., Farquhar, J. & Shearer, C. Anomalous 33S in the Lunar Mantle. *Journal of Geophysical Research: Planets* **128**, e2022JE007597 (2023).
65. Boehler, R. Melting of the FeFeO and the FeFeS systems at high pressure: Constraints on core temperatures. *Earth and Planetary Science Letters* **111**, 217–227 (1992).
66. Forrest, J. & Newman, L. Sampling and analysis of atmospheric sulfur compounds for isotope ratio studies. *Atmospheric Environment (1967)* **7**, 561–573 (1973).
67. Labidi, J., Cartigny, P., Birck, J. L., Assayag, N. & Bourrand, J. J. Determination of multiple sulfur isotopes in glasses: A reappraisal of the MORB δ34S. *Chemical Geology* **334**, 189–198 (2012).
68. Dottin, J. W., Labidi, J., Lekic, V., Jackson, M. G. & Farquhar, J. Sulfur isotope characterization of primordial and recycled sources feeding the Samoan mantle plume. *Earth and Planetary Science Letters* **534**, 116073 (2020).
69. Crowe, D. E. & Vaughan, R. G. Characterization and use of isotopically homogeneous standards for in situ laser microprobe analysis of 34S/32 S ratios. *American Mineralogist* **81**, 187–193 (1996).

70. LaFlamme, C. *et al.* In situ multiple sulfur isotope analysis by SIMS of pyrite, chalcopyrite, pyrrhotite, and pentlandite to refine magmatic ore genetic models. *Chemical Geology* **444**, 1–15 (2016).

71. Ding, T. *et al.* Calibrated sulfur isotope abundance ratios of three IAEA sulfur isotope reference materials and V-CDT with a reassessment of the atomic weight of sulfur. *Geochimica et Cosmochimica Acta* **65**, 2433–2437 (2001).

72. Liu, L., Mavrogenes, J., Holden, P. & Ireland, T. Quadruple sulfur isotopic fractionation during pyrite desulfidation to pyrrhotite. *Geochimica et Cosmochimica Acta* **273**, 354–366 (2020).

73. Brandon, A. D., Walker, R. J., Morgan, J. W. & Goles, G. G. Re-Os isotopic evidence for early differentiation of the Martian mantle. *Geochimica et Cosmochimica Acta* **64**, 4083–4095 (2000).

74. Brandon, A. D. *et al.* Evolution of the martian mantle inferred from the 187Re–187Os isotope and highly siderophile element abundance systematics of shergottite meteorites. *Geochimica et Cosmochimica Acta* **76**, 206–235 (2012).

75. SULFUR IN ACHONDRITIC METEORITES - Gibson - 1985 - Meteoritics - Wiley Online Library. https://onlinelibrary.wiley.com/doi/abs/10.1111/j.1945-5100.1985.tb00046.x.

76. Lodders, K. A survey of shergottite, nakhlite and chassigny meteorites whole-rock compositions. *Meteoritics & Planetary Science* **33**, A183–A190 (1998).

77. Petrology and chemistry of the new shergottite Dar al Gani 476 - ZIPFEL - 2000 - Meteoritics & Planetary Science - Wiley Online Library. https://onlinelibrary.wiley.com/doi/abs/10.1111/j.1945-5100.2000.tb01977.x.

78. Shirai, N. & Ebihara, M. Chemical characteristics of a Martian meteorite, Yamato 980459. *Antarctic Meteorite Research* **17**, 55 (2004).

79. Aoudjehane, H. C. *et al.* Tissint Martian Meteorite: A Fresh Look at the Interior, Surface, and Atmosphere of Mars. *Science* **338**, 785–788 (2012).

80. Brennan, M. C., Fischer, R. A., Nimmo, F. & O'Brien, D. P. Timing of Martian core formation from models of Hf–W evolution coupled with *N*-body simulations. *Geochimica et Cosmochimica Acta* **316**, 295–308 (2022).

81. Zelenski, M., Kamenetsky, V. S., Nekrylov, N. & Kontonikas-Charos, A. High Sulfur in Primitive Arc Magmas, Its Origin and Implications. *Minerals* **12**, 37 (2022).

82. Wang, Z. & Becker, H. Chalcophile elements in Martian meteorites indicate low sulfur content in the Martian interior and a volatile element-depleted late veneer. *Earth and Planetary Science Letters* **463**, 56–68 (2017).

Acknowledgments

Funding: This research was funded by Brown university (JD, KP) and NASA Solar System Exploration Virtual Institute (# 22-SSERVI4_2-0009 to JD and 22-SSERVI4_2-0012 to JD and HF).

Author contributions:

KP: Conceptualisation, methodology, investigation, visualisation, writing - original draft and review and editing.

JD: Conceptualisation, methodology, supervision, investigation, visualisation, writing - original draft and review and editing.

HF: Investigation, visualisation, writing - original draft and review and editing.

BM: Methodology, investigation, review and editing.

NC: Methodology, investigation, review and editing.

NH: Methodology, investigation, review and editing.

JCA: Investigation, review and editing.

GI: Investigation, review and editing.

AI: Review and editing.

CS: Review and editing.

HBF: Review and editing.

SO: Review and editing.

Competing interest: All others declare they have no competing interests.

Data and material availability: All the elemental compositions and sulfur isotopic data for the analysed sulfides in this study are available on Zenodo, the main text and the supplementary materials. (https://doi.org/10.5281/zenodo.18760943)

Figures and Tables

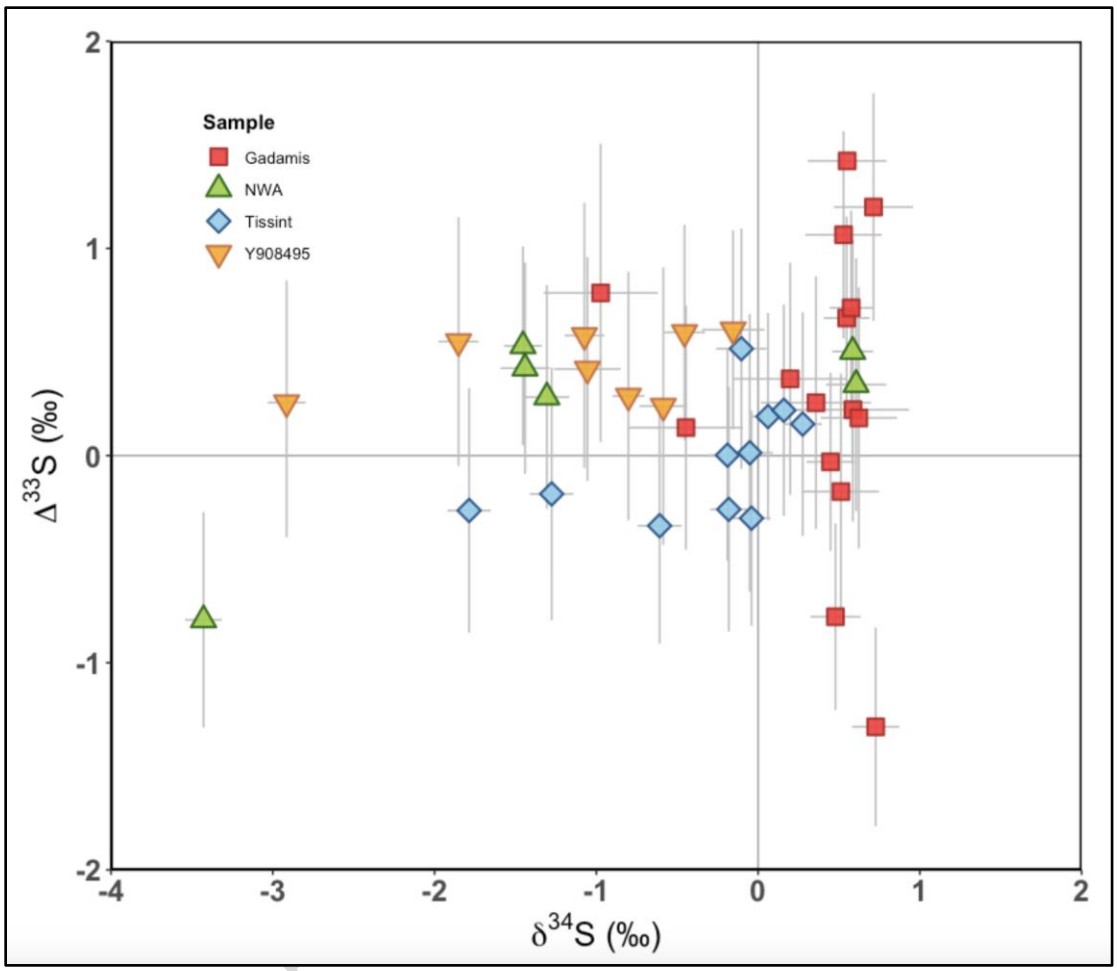

Figure 1. In-situ triple sulfur isotope compositions measured in shergottites. Red squares represent Gadamis 001, blue diamonds are sulfides in Tissint, green triangles are NWA 11300, and orange inverted triangles represent Y980459. The $\delta^{34}S$ values range from 2.91 ± 0.12 to –0.15 ± 0.19 ‰ (2$\boldsymbol{\sigma}$) in Y98, -1.79 ± 0.13 ‰ to 0.28 ± 0.12 ‰ (2$\boldsymbol{\sigma}$) in Tissint, -0.97 ± 0.35 ‰ (2$\boldsymbol{\sigma}$) to -0.73 ‰ ± 0.15 (2$\boldsymbol{\sigma}$) in Gadamis 001, and –3.43 ± 0.27 ‰ (2$\boldsymbol{\sigma}$) to 0.61 ± 0.19 ‰ (2$\boldsymbol{\sigma}$) in NWA 11300. The $\Delta^{33}S$ values range from 0.24 ± 0.67 to 0.61 ± 0.48 ‰ (2$\boldsymbol{\sigma}$) in Y98, –0.34 ± 0.57 ‰ to 0.52 ± 0.58 ‰ (2$\boldsymbol{\sigma}$) in Tissint, –1.31 ± 0.48 ‰ to 1.42 ± 0.64 ‰ (2$\boldsymbol{\sigma}$) in Gadamis 001, and –0.79 ± 0.52 ‰ (2$\boldsymbol{\sigma}$) to 0.53 ± 0.48 ‰ (2$\boldsymbol{\sigma}$) in NWA 11300.

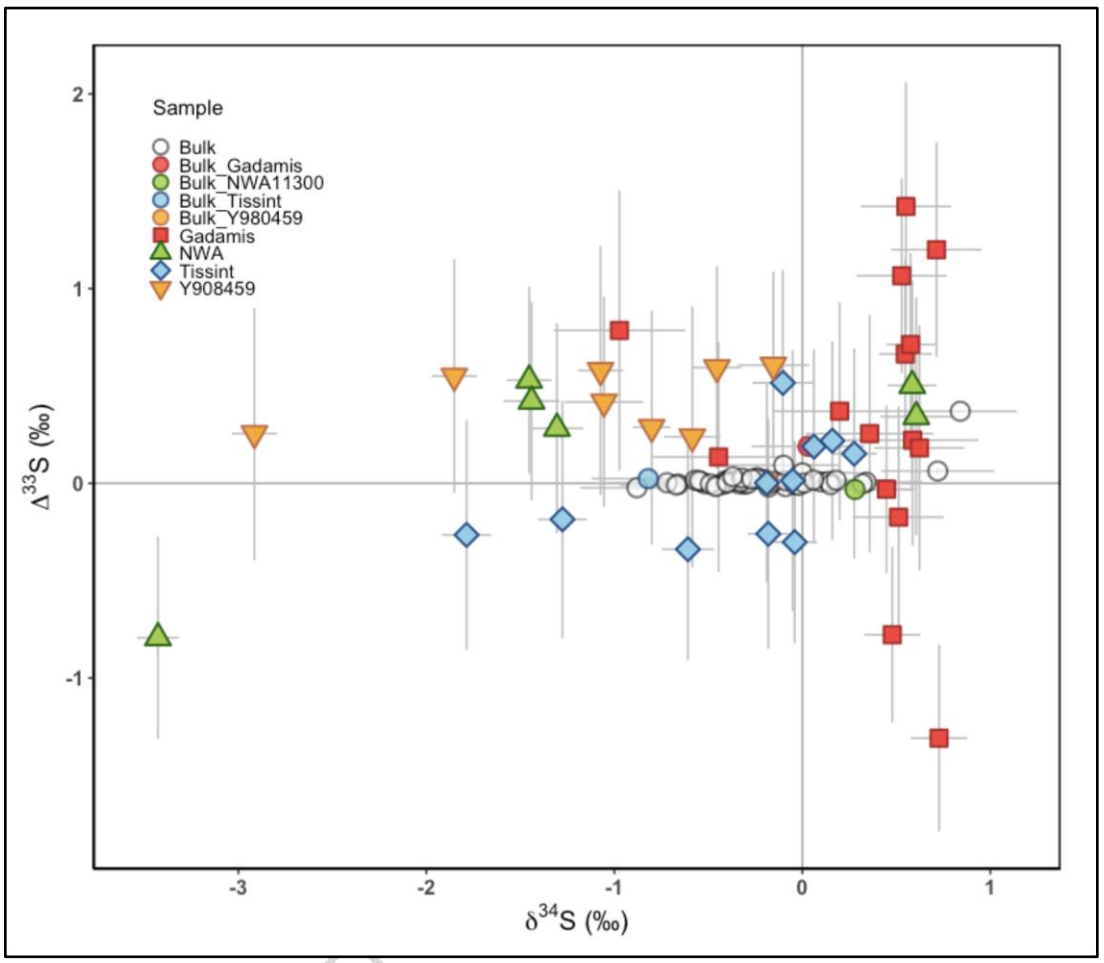

Figure 2. Bulk and SIMS derived sulfur isotope data ($\delta^{34}S$ and $\Delta^{33}S$) of Martian Meteorites. SIMS sulfur isotope data from Y98, Tissint, NWA 11300, and Gadamis 001, superimposed on existing bulk sulfur isotope (represented as white circles) data from shergottites [18,21,22]. Bulk sulfur isotope techniques, which yield $\delta^{34}S$ values of –0.88 to +0.84‰ (±0.3‰, 2 S.D.) and $\Delta^{33}S$ values ranging from –0.032 to +0.37‰ (±0.016‰, 2 S.D.) [18,21,22]. SIMS data exhibit extreme heterogeneity in $\delta^{34}S$ (~ –3.5 to +0.7‰) and $\Delta^{33}S$ (–1.3 to +1.4‰)

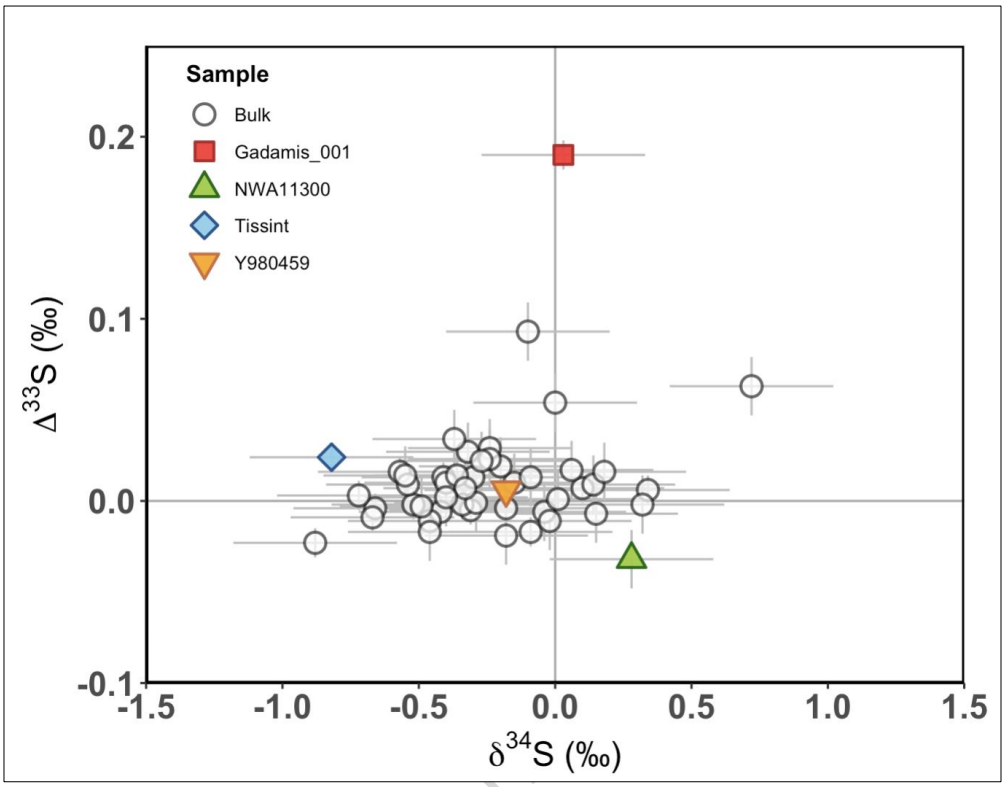

Figure 3. A compilation of bulk sulfide sulfur isotope compositions from shergottites. Plotted are $\Delta^{33}S$ vs. $\delta^{34}S$ values compiled from [18,21,22]. Bulk sulfur isotope techniques, which yield $\delta^{34}S$ values of –0.88 to +0.84‰ (±0.3‰) and $\Delta^{33}S$ values ranging from –0.032 to +0.37‰ (±0.016‰).[18,21,22] This figure illustrates that although most shergottites exhibit $\Delta^{33}S$ values close to 0 ‰, there are a few exceptions. Gadamis 001 has the largest $\Delta^{33}S$ value, while NWA 11300 is the only shergottite with a negative $\Delta^{33}S$ anomaly.

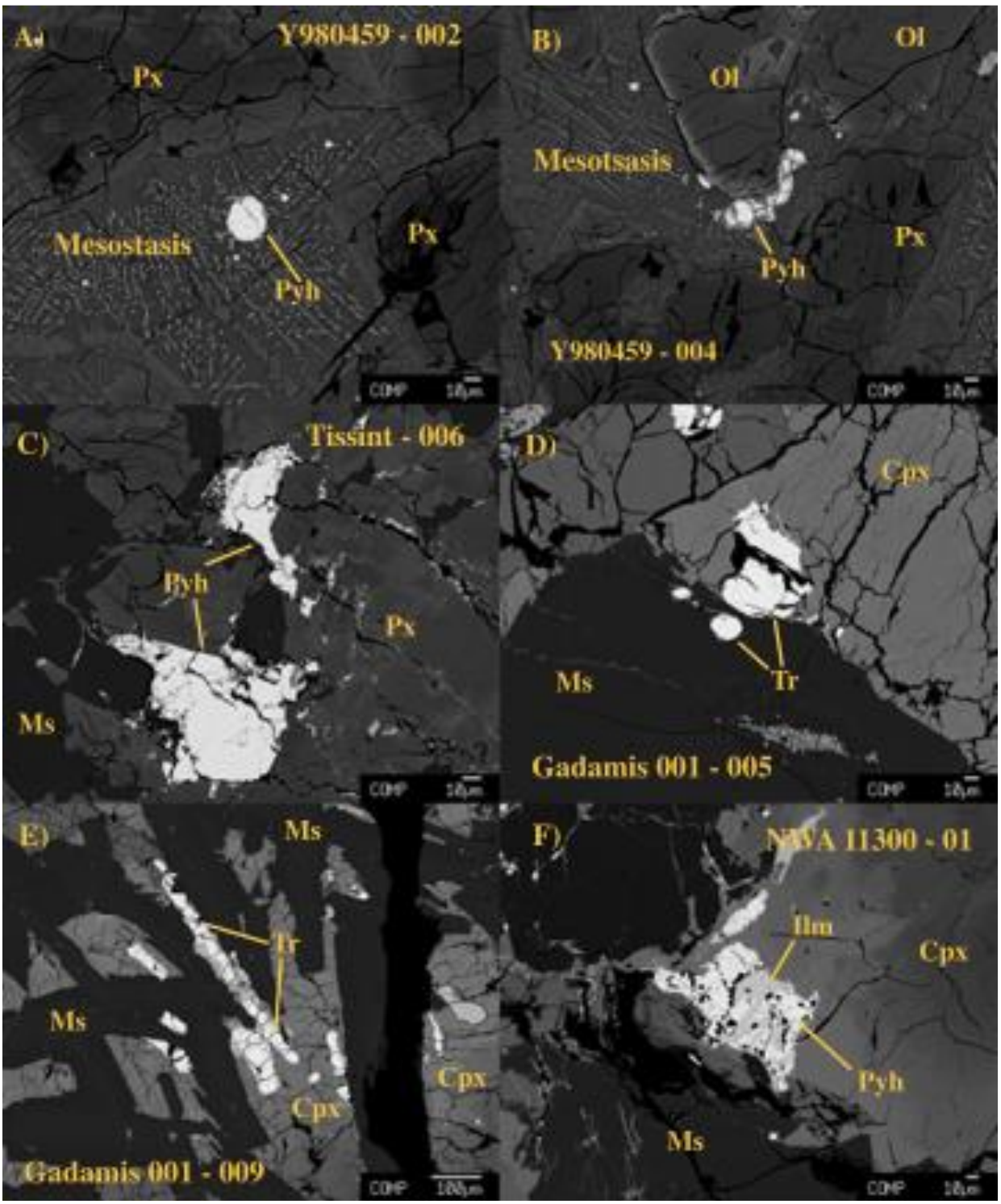

Figure 4. Backscattered electron (BSE) images of representative sulfide-bearing assemblages. (A, B) Yamato 980459, (C) Tissint, (D, F) Gadamis 001, and (E) NWA 11300. The images highlight sulfides that exhibit the largest sulfur isotope anomalies in each sample. Abbreviations: Ol = olivine; Px = pyroxene; Cpx = clinopyroxene; Pyh = pyrrhotite; Ms = maskelynite; Ilm = ilmenite; Tr = troilite.

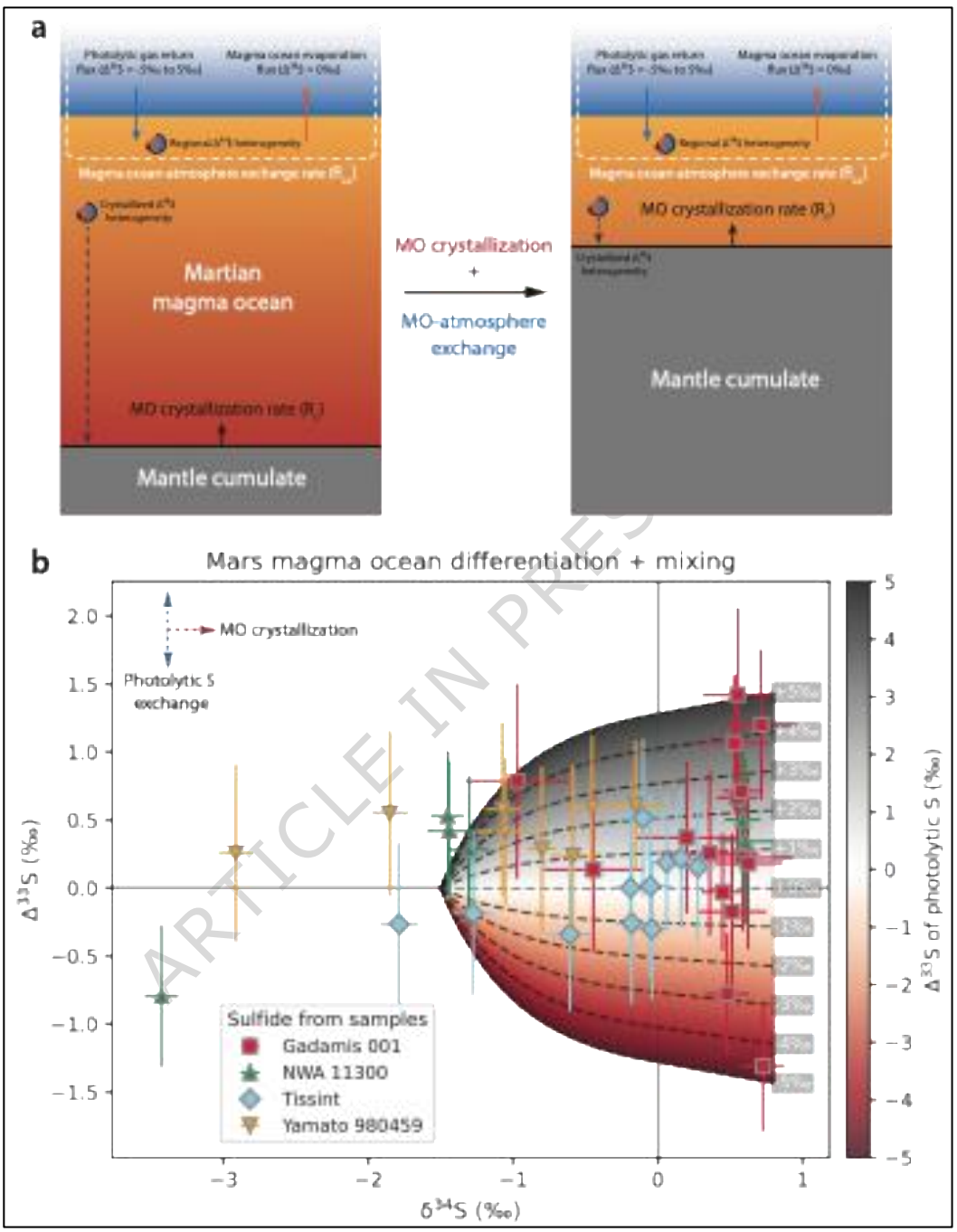

Figure 5. Martian magma-ocean fractionation-mixing model explaining the linked $\delta^{34}S$ and $\Delta^{33}S$ variations. (a) Schematic model of magma-ocean (MO) differentiation and MO-atmosphere exchange. As the MO crystallizes, photolytic sulfur with variable $\Delta^{33}S$ anomalies continues to form in the atmosphere and exchange with the MO, generating local $\Delta^{33}S$ heterogeneities within it. Progressive crystallisation can preserve these local $\Delta^{33}S$ variations in the solidifying mantle cumulates. Subsequent partial melting of these heterogeneous cumulates can produce magmas (shergottites) exhibiting diverse $\Delta^{33}S$ signatures. **(b) Quantitative MO differentiation-exchange model.** The model starts with an initial bulk-silicate Mars composition of $\delta^{34}S$ = -1.5‰ and $\Delta^{33}S$ = 0‰. During MO differentiation, sulfur

enrichment and sulfide saturation cause isotopically heavier $\delta^{34}S$ values to develop in the crystallizing cumulates. Hence, the increasing $\delta^{34}S$ trend represents progressively heavier source compositions (up to ~0.5‰) in later-stage partial melts. The colour field indicates the modelled $\Delta^{33}S$ of the mantle cumulates formed from different local MO reservoirs, each resulting from continuous mixing between MO sulfur and photolytically fractionated sulfur returned from the atmosphere (colour bar shows the $\Delta^{33}S$ of the photolytic input). With ongoing crystallisation, these MO local reservoirs preserve heterogeneous $\Delta^{33}S$ signatures in the mantle cumulates that ultimately source shergottites. Black dashed lines show mixing trajectories for different assumed $\Delta^{33}S$ values of the photolytic sulfur component (labelled). The widening $\Delta^{33}S$ range toward higher $\delta^{34}S$ values illustrates how $\Delta^{33}S$ variabilities-acquired in the MO, recorded in cumulates, and inherited by partial melts-increase as MO differentiation and atmospheric exchange proceed simultaneously. Dashed arrows in the upper left corner indicate the directions of $\delta^{34}S$ and $\Delta^{33}S$ fractionation in the mantle cumulates (and their derived partial melts) associated with these two processes.

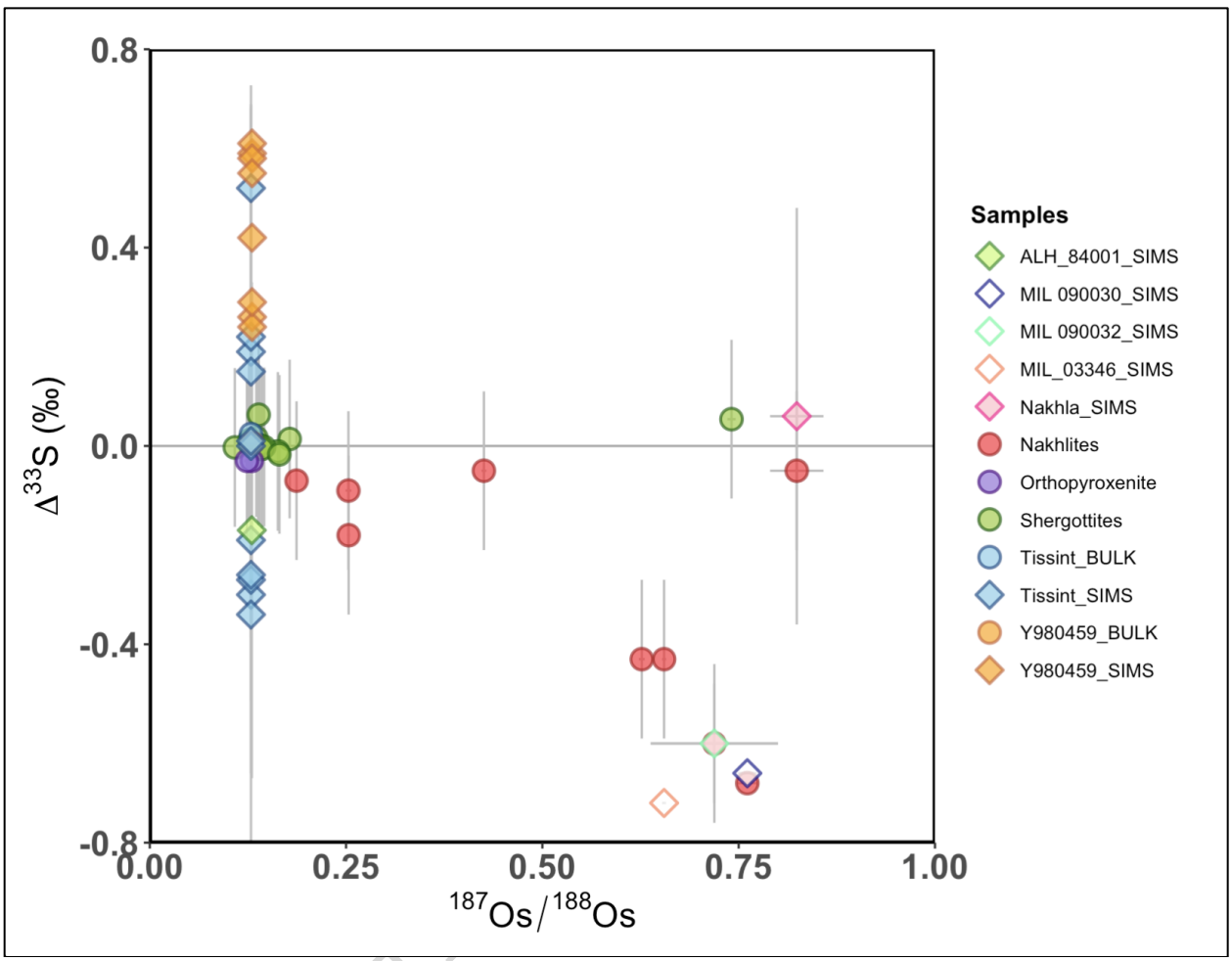

Figure 6. Plot of $\Delta^{33}S$ vs. $^{187}Os/^{188}Os$. Bulk $\Delta^{33}S$ data acquired from [18,21,22] and $^{187}Os/^{188}Os$ data from [26,28,73,74]. Nakhlites exhibit a negative correlation between $\Delta^{33}S$ and $^{187}Os/^{188}Os$, suggesting crustal assimilation. In contrast, no clear relationship is observed for shergottites, which maintain low $^{187}Os/^{188}Os$ values even in cases with anomalous $\Delta^{33}S$, indicating a lack of crustal assimilation.

Table 1. Cu, S, Fe, Zn, Ti and Ni concentrations in weight % of sulfides analysed in all samples.

No.	Samples	Cu	S	Fe	Zn	Ti	Ni	Total
1	Tissint-1_1	0.34	38.75	55.48	0.15	0.01	6.18	100.91
2	Tissint-1_2	0.42	38.76	54.79	0.03	0.02	6.19	100.21
3	Tissint-3_1	0.02	38.97	59.94	0.14	0.04	0.84	99.96
4	Tissint-5_1	0.00	38.80	59.38	0.00	0.05	1.92	100.15
5	Tissint-5_2	0.14	39.05	59.05	0.11	0.15	1.68	100.18
6	Tissint-6_1	0.00	38.66	59.62	0.37	0.04	1.76	100.45
7	Tissint-6_3	0.00	38.87	59.33	0.00	0.02	1.78	100.00
8	Tissint-7_1	0.00	38.53	59.44	0.07	0.04	2.22	100.30
9	Tissint-8_1	1.46	38.65	56.91	0.00	0.00	2.98	100.00
10	Tissint-9_1	0.00	38.90	59.91	0.00	0.01	1.31	100.13
11	Tissint-9_2	0.00	38.78	59.72	0.00	0.02	1.33	99.85
12	Yamato-1_1	0.00	37.97	61.54	0.00	0.07	0.28	99.85
13	Yamato-2_1	0.00	38.63	61.31	0.00	0.03	0.69	100.66
14	Yamato-4_1	0.00	39.75	56.38	0.00	0.05	4.24	100.42
15	Yamato-6_1	0.00	34.47	61.08	0.00	0.04	1.59	97.18
16	Yamato-7_1	0.00	40.69	52.70	0.00	0.05	6.94	100.38
17	Yamato-8_1	0.00	34.34	62.68	0.00	0.08	0.22	97.33
18	Yamato-9_1	0.00	36.94	59.25	0.00	0.08	1.64	97.91
19	Yamato-10_1	0.00	36.06	61.42	0.00	0.02	0.72	98.22
20	Gadamis 001-1_1	0.00	38.06	63.86	0.27	0.02	0.04	102.25
21	Gadamis 001-2_1	0.00	38.43	63.23	0.01	0.01	0.03	101.71
22	Gadamis 001-2_3	0.00	38.60	63.49	0.13	0.00	0.04	102.26
23	Gadamis 001-4_1	0.00	38.02	63.26	0.15	0.00	0.01	101.45
24	Gadamis 001-4_2	0.00	38.10	63.01	0.19	0.00	0.04	101.34
25	Gadamis 001-5_1	0.00	38.28	62.60	0.24	0.00	0.03	101.15
26	Gadamis 001-5_2	0.34	38.18	62.18	0.02	0.00	0.07	100.79
27	Gadamis 001-6_1	0.00	38.53	62.98	0.01	0.00	0.06	101.58
28	Gadamis 001-6_2	0.01	38.38	63.21	0.25	0.00	0.05	101.90
29	Gadamis 001-7_1	0.00	38.36	63.23	0.10	0.00	0.06	101.75
30	Gadamis 001-8_1	0.00	38.29	62.84	0.05	0.00	0.06	101.24
31	Gadamis 001-9_1	0.00	37.91	63.70	0.01	0.02	0.05	101.68
32	Gadamis 001-9_2	0.02	38.56	63.18	0.17	0.00	0.03	101.96
33	Gadamis 001-10_1	0.14	38.23	62.97	0.00	0.00	0.07	101.41
34	Gadamis 001-10_2	0.00	38.72	62.92	0.00	0.00	0.03	101.67
35	NWA 11300-1_1	0.00	37.14	62.79	0.13	0.00	0.30	100.36
36	NWA 11300-1_2	0.06	37.43	61.94	0.32	0.00	0.48	100.23

37	NWA 11300-2_1	0.00	36.39	61.50	0.13	0.03	0.35	98.40
38	NWA 11300-2_2	0.00	37.93	61.99	0.01	0.04	0.37	100.34
39	NWA 11300-4_1	0.00	38.38	62.24	0.09	0.00	0.35	101.07
40	NWA 11300-4_2	0.00	37.62	61.64	0.00	0.00	0.37	99.64

Table 2. Sulfur isotope compositions ($\delta^{34}S$ and $\Delta^{33}S$) with 2σ error for all analysed sulfides.

No.	Samples	$\delta^{34}S$	2σ	$\Delta^{33}S$	2σ
1	Tissint-1_1	0.06	0.10	0.19	0.50
2	Tissint-1_2	-0.04	0.12	-0.30	0.52
3	Tissint-3_1	-0.19	0.12	0.00	0.51
4	Tissint-5_1	0.16	0.12	0.22	0.51
5	Tissint-5_2	-1.28	0.13	-0.19	0.61
6	Tissint-6_1	0.28	0.12	0.15	0.54
7	Tissint-6_2	-0.10	0.16	0.52	0.58
8	Tissint-7_1	-0.61	0.14	-0.34	0.57
9	Tissint-8_1	-1.79	0.13	-0.27	0.59
10	Tissint-9_1	-0.18	0.11	-0.26	0.59
11	Tissint-9_2	-0.05	0.14	0.01	0.67
12	Yamato-1_1	-1.06	0.21	0.42	0.54
13	Yamato-2_1	-0.45	0.13	0.59	0.52
14	Yamato-4_1	-0.15	0.19	0.61	0.48
15	Yamato-6_1	-2.91	0.12	0.26	0.65
16	Yamato-7_1	-1.07	0.12	0.58	0.64
17	Yamato-8_1	-1.85	0.12	0.55	0.60
18	Yamato-9_1	-0.59	0.15	0.24	0.67
19	Yamato-10_1	-0.80	0.10	0.29	0.60
20	Gadamis 001-1_1	0.20	0.35	0.37	0.56
21	Gadamis 001-2_1	-0.97	0.35	0.79	0.72
22	Gadamis 001-2_3	-0.45	0.35	0.14	0.59
23	Gadamis 001-4_1	0.59	0.35	0.22	0.54
24	Gadamis 001-4_2	0.36	0.34	0.26	0.61
25	Gadamis 001-5_1	0.73	0.15	-1.31	0.48
26	Gadamis 001-5_2	0.48	0.15	-0.78	0.45
27	Gadamis 001-6_1	0.55	0.14	0.66	0.49
28	Gadamis 001-6_2	0.45	0.15	-0.03	0.43
29	Gadamis 001-7_1	0.58	0.13	0.71	0.47
30	Gadamis 001-8_1	0.62	0.24	0.18	0.63
31	Gadamis 001-9_1	0.55	0.24	1.42	0.64
32	Gadamis 001-9_2	0.53	0.24	1.07	0.50
33	Gadamis 001-10_1	0.51	0.24	-0.17	0.57
34	Gadamis 001-10_2	0.71	0.24	1.20	0.55
35	NWA 11300-1_1	-1.45	0.12	0.53	0.48
36	NWA 11300-1_2	-3.43	0.11	-0.79	0.52
37	NWA 11300 -2_1	0.61	0.19	0.34	0.61

38	NWA 11300 -2_2	0.58	0.13	0.50	0.54
39	NWA 11300 -4_1	-1.44	0.15	0.42	0.51
40	NWA 11300 -4_2	-1.31	0.14	0.28	0.54

Table 3. Measured sulfur isotope compositions ($\delta^{34}S$ and $\Delta^{33}S$) of the standards analysed in this study ($\pm 2\sigma$) compared to the accepted values. Pyrite and chalcopyrite are abbreviated py and ccp, respectively.

Standard	Measured $\delta^{34}S \pm 2\sigma$	Accepted $\delta^{34}S \pm 2\sigma$	Measured $\Delta^{33}S \pm 2\sigma$	Accepted $\Delta^{33}S \pm 2\sigma$
Sierra (py)	2.17 ± 0.10	2.17 ± 0.08†	-0.03 ± 0.10	− 0.02 ± 0.02†
Nifty-b (ccp) [70]	-3.58 ± 0.08	-3.58 ± 0.14 †	-0.07 ± 0.10	− 0.06 ± 0.06†
Anderson[69]	1.4 ± 0.14	1.4 ± 0.10†	0.00 ± 0.12	0.00 ± 0.028†
Lab_Std	17.77 ± 0.14	17.77 ± 0.10†	0.04 ± 0.11	0.04 ± 0.014†
AMNH 112266	2.40 ± 0.14	2.42 ± 0.10†	0.09 ± 0.10	0.08 ± 0.006†
AMNH 26170	11.8 ± 0.10	11.8 ± 0.10†	-0.03 ± 0.11	0.06 ± 0.012†

†Uncertainty reflects standard deviation from repeat measurements.

Editorial summary:
In situ S isotope analyses of Martian shergottites reveal extreme $\Delta^{33}S$ heterogeneity at the mineral scale, indicating that mass-independent S signatures were incorporated into the mantle early via atmosphere–mantle exchange during magma ocean evolution

Peer review information:

Communications Earth and Environment thanks Xiaoping Xia and the other, anonymous, reviewer(s) for their contribution to the peer review of this work. Primary Handling Editors: Ke Zhu and Joe Aslin. A peer review file is available.